

Supporting Information for “Synchronous emplacement of the anorthosite xenolith-bearing Beaver River diabase and one of the largest lava flows on Earth”

Yiming Zhang, Nicholas L. Swanson-Hysell, Mark D. Schmitz, James D. Miller Jr., Margaret S. Avery

Field observations on sampled Beaver River diabase and anorthosite xenoliths

The measured dimensions of each anorthosite xenolith sampled for paleomagnetism study during the fieldwork of this study are summarized in Table DR1. The estimated distance from each anorthosite site to the closest diabase site are also shown in the table.

Table DR1. Summary of anorthosite xenolith dimensions and their approximate distance from the closest diabase site.

Anorthosite site	Xenolith dimension (m)	Closest diabase site	Distance from anorthosite site to closest diabase site (m)
AX1	3.1 X 1.3	BD1	<5
AX2	4 X 15 X 30	BD1	<5
AX3	100 X 30	BD2	200
AX4	20 X 10	BD2	50
AX5	0.5 X 0.45	BD2	20
AX6	0.7 X 0.6	BD2	20
AX7	0.8 X 0.5	BD2	20
AX8	0.4 X 0.25	BD2	20
AX9	0.3 X 0.6	BD2	20
AX10	0.47 X 0.47	BD2	20
AX11	120 X 30	BD3	150
AX12	31 X 5	BD4	32
AX13	36 X 8	BD3	30
AX14	10 X 3	BD4	150
AX15	5.8 X 5.5	BD5	<5
AX16	27.5 X 5	BD5	25
AX17	4.2 X 2	BD5	<5
AX18	15.6 X 3	BD5	<5
AX19	7.5 X 2.9	BD6	9
AX20	8.1 X 6.5	BD7	<5
AX21	3.2 X 1.2	BD7	300
AX22	5 X 12 X 10	BD10	<10

ID-TIMS U-Pb zircon geochronology methods

U-Pb dates were obtained by chemical abrasion isotope dilution thermal ionization mass spectrometry (ID-TIMS) in the Boise State University (BSU) Isotope Geology Laboratory (Table

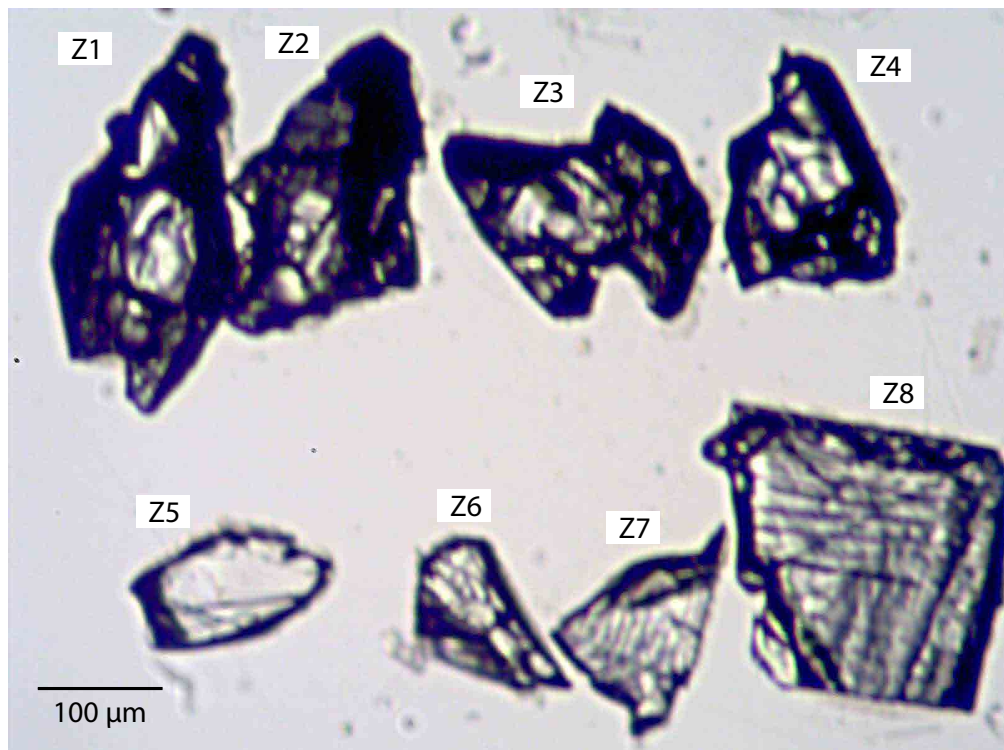


Figure SI1. Image of individual zircons used for ID-TIMS U-Pb geochronology from sample MS99033. Zircons (z1-z4) are subhedral to anhedral crystals and (z5-z8) are platy fragments.

DR2; Fig. SI1).

Zircon were separated from the bulk rock sample using a sledge, Retsch DM200 disc mill, 500 μm sieve, Wilfley Shaker Table, LB-1 Frantz magnetic separator, and methylene iodide heavy liquid. Heavy separates were annealed at 900°C for 48 to 60 hours in quartz crucibles in a muffle furnace. Individual zircons were chemically abraded. Chemical abrasion was carried out by transferring zircons to 3 ml Teflon Perfluoroalkoxy alkane (PFA) beakers in which they were rinsed in 3.5 M HNO₃ and ultrapure H₂O prior to loading into 300 μl Teflon PFA microcapsules. Fifteen microcapsules were placed in a large-capacity Parr vessel and the zircon partially dissolved in 120 μl of 29 M HF for 12 hours at 190°C. Zircons were returned to 3 ml Teflon PFA beakers, HF was removed, and zircons were immersed in 3.5 M HNO₃, ultrasonically cleaned for an hour, and fluxed on a hotplate at 80°C for an hour. The HNO₃ was removed and zircon was rinsed twice in ultrapure H₂O before being reloaded into the 300 μl Teflon PFA microcapsules (rinsed and fluxed in 6 M HCl during sonication and washing of the zircons) and spiked with the ²³³U-²³⁵U-²⁰⁵Pb BSU tracer solution (BSU1B). Zircons were dissolved in Parr vessels in 120 μl of 29 M HF at 220°C for 48 hours, dried to fluorides, and re-dissolved in 6 M HCl at 180°C overnight. Pb and U were separated from the zircon matrix using an HCl-based anion-exchange chromatographic procedure (Krogh, 1973), eluted together and dried with 2 μl of 0.05 N H₃PO₄.

Pb and U were loaded on a single outgassed Re filament in 5 μl of a silica-gel/phosphoric acid mixture (Gerstenberger and Haase, 1997), and Pb and U isotopic measurements made on a GV Isoprobe-T multicollector thermal ionization mass spectrometer equipped with an ion-counting Daly detector. Pb isotopes were measured by peak-jumping all isotopes on the Daly detector for

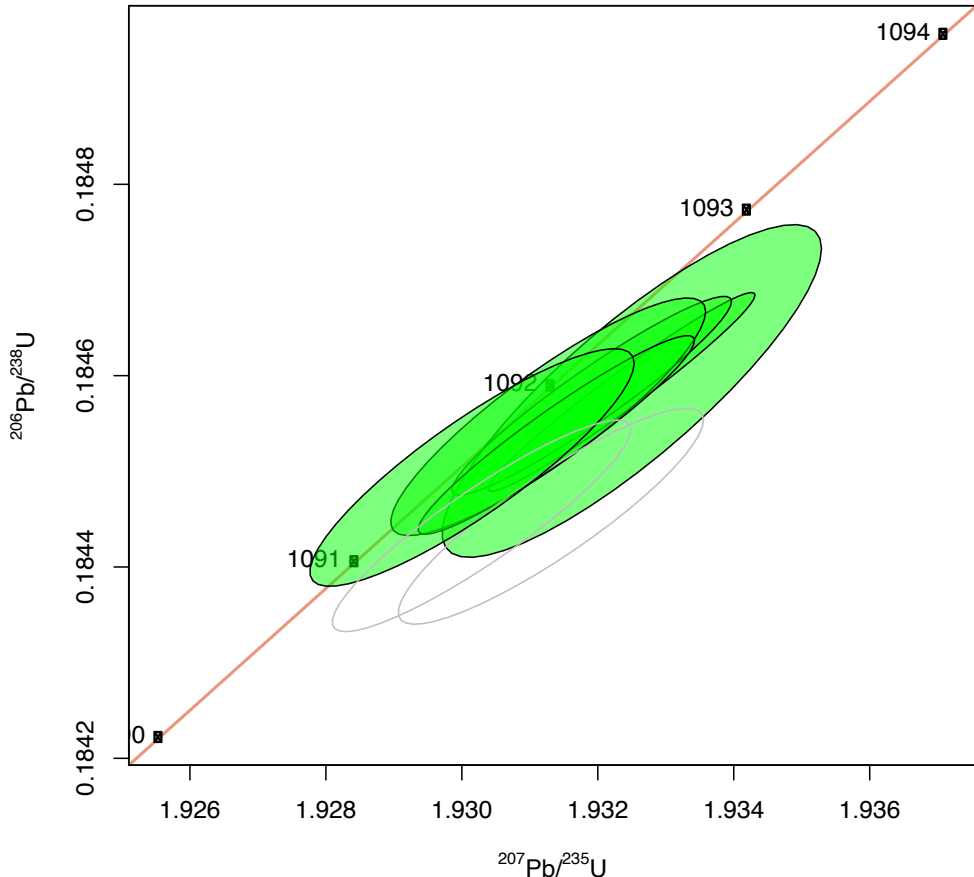


Figure SI2. U-Pb concordia plots for the new zircon dates from anorthosite xenoliths AX16, geochronology sample MS99033. The ellipses represent 2σ analytical uncertainty on individual zircon dates. Green filled ellipses are analyses included in the $^{206}\text{Pb}/^{238}\text{U}$ weighted mean dates while the grey ellipses are those that were excluded.

190 cycles with a mass bias correction of $0.16 \pm 0.03\%$ /a.m.u. (1σ). Transitory isobaric interferences due to high-molecular weight organics, particularly on ^{204}Pb and ^{207}Pb , disappeared within 30-45 cycles, while ionization efficiency averaged 104 cps/pg of each Pb isotope. Linearity (to $\geq 1.4 \times 10^6$ cps) and the associated deadtime correction of the Daly detector were determined by analysis of NBS982. Uranium was analyzed as UO_2^+ ions in static Faraday mode on 10^{12} ohm resistors for up to 300 cycles, and corrected for isobaric interference of $^{233}\text{U}^{18}\text{O}^{16}\text{O}$ on $^{235}\text{U}^{16}\text{O}^{16}\text{O}$ with an $^{18}\text{O}/^{16}\text{O}$ of 0.00206. Ionization efficiency averaged 20 mV/ng of each U isotope. U mass fractionation was corrected using the $^{233}\text{U}/^{235}\text{U}$ ratio of the BSU1B tracer.

Zircon geochemistry, cathodoluminescence images, and photomicrograph

An additional 15 zircons extracted from sample MS99033 were analyzed by laser ablation inductively coupled plasma mass spectrometry (LA-ICPMS) using a ThermoElectron, iCAP-RQ, single quadrupole ICPMS and a Teledyne (Photon Machines) Analyte Excite+ 193 nm excimer Analyte laser with a HelEx ablation cell at BSU. Analytical protocols, standard materials, and data reduction software developed at BSU were used for acquisition and calibration of U-Pb dates

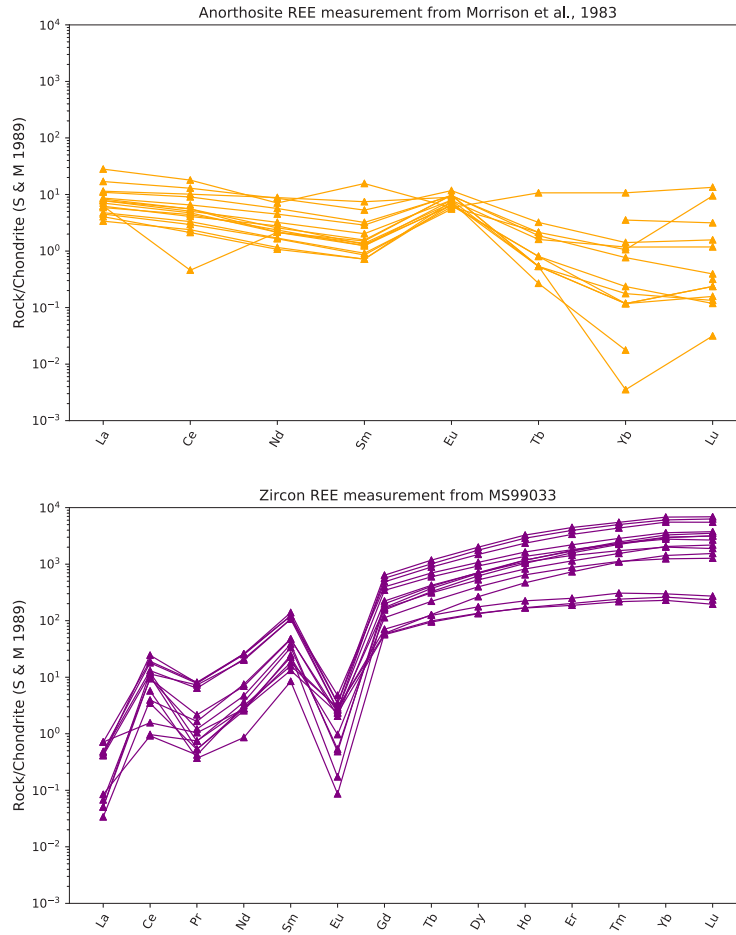


Figure SI3. Top: Rare earth element (REE) analyses on anorthosite xenoliths and plagioclase crystals by Morrison et al. (1983); Bottom: REE analyses on 15 zircons from geochronology sample MS99033 via inductively coupled plasma mass spectrometry.

and a suite of high field strength elements (HFSE) and rare earth elements (REE). Zircon were ablated with a 25 μm diameter laser spot using fluence and pulse rates of $\sim 2.5 \text{ J/cm}^2$ and $\sim 5 \text{ Hz}$, respectively, during a 20-second analysis excavating a pit 25 μm deep. Ablated material was carried to the nebulizer flow of the plasma by a 1.2 L/min He gas stream. Total sweep duration is 895 ms, and quadrupole dwell times were 5 ms for Si and Zr, 40 ms for ^{202}Hg , ^{204}Pb , ^{208}Pb , ^{232}Th , and ^{238}U , 80 ms for ^{206}Pb , 200 ms for ^{49}Ti and ^{207}Pb , and 10 ms for all other HFSE and REE. Background count rates were obtained prior to each spot analysis and subtracted from the raw count rate for each analyte. Concentrations were calculated using background-subtracted count rates internally normalized to ^{29}Si and calibrated with the primary standards NIST SRM-610 and -612 glasses. Ablation pits that intersected mineral inclusions were identified based on Ti and P spikes. The Ti-in-zircon thermometer was calculated using an average TiO_2 activity value of 0.7 in crustal rocks (Watson et al., 2006) and an average SiO_2 activity value of 1.0 (Ferry and Watson, 2007).

MS99-33 Anorthosite Xenolith, Beaver River Diabase Hwy 61 roadcut at Silver Bay, MN CL, 500x 04/26/2021

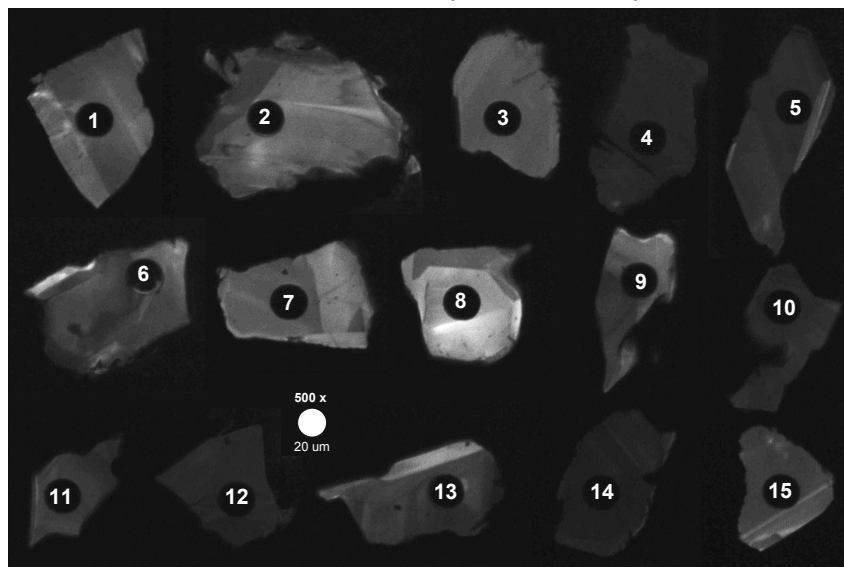


Figure SI4. Cathodoluminescence (CL) image montage of the 15 laser-ablated zircons. Immediately apparent are sharp boundaries between zones of differing CL response within many crystals. The bright zoning in grain 15 has a thickness of ~2 μm . Note that grain 1 (corresponding to spot 1) has a platy morphology, while the rest are subhedral to anhedral zircons.

The resulting zircon REE diagrams are shown in Fig. SI3. All zircons analyzed show a strong negative Eu anomaly on chondrite-normalized REE diagrams (Sun and McDonough, 1989). This result is consistent with the zircons having crystallized from a liquid that has had significant plagioclase extraction. On the other hand, REE analyses on anorthosite xenoliths whole rocks and plagioclase crystals from (Morrison et al., 1983) show positive Eu anomaly. The opposite Eu anomalies from plagioclase and zircons allow for an interpretation that they crystallized from a same parent magma. The cathodoluminescence images of the 15 laser-ablated zircons are shown in Fig. SI4.

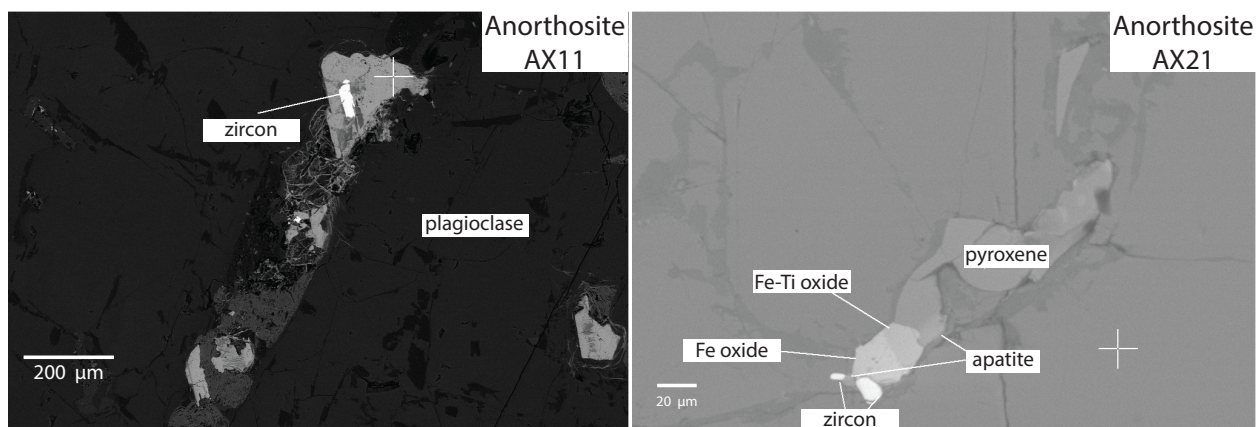


Figure SI5. Back scattered electron (BSE) images of anorthosite xenoliths. Subhedral to anhedral zircons form next to mafic melt pockets.

Fig. SI5 shows subhedral and anhedral zircons in anorthosite xenoliths AX11 and AX 21 in back scattered electron (BSE) images of anorthosite thin sections. All zircons found are residing next to interstitial mafic melt pockets. This is consistent with the interpretation of a zircon formation from interstitial melt liquids preserved in plagioclase mush.

Evaluating Pb diffusive loss

Our thermal history modeling indicates that the xenoliths could have equilibrated to the temperature of the olivine tholeiitic magma (~ 1100 to 1200°C) and remained at that temperature for more than 100 years in the diabase sill interior. Following the Pb diffusion rate from Cherniak and Watson (2001), we plotted the temperature and time relationships for diffusing out Pb from zircons with effective radii of $60 \mu\text{m}$ in Fig. SI6. The model shows that if a temperature of 1200°C is sustained for ~ 10 thousand years (before the final cooling after diabase emplacement), $\sim 90\%$ of Pb will diffuse out of a $\sim 120 \mu\text{m}$ diameter zircon. Assuming that the zircons from MS99033 crystallized at 1096 Ma and suffered various degrees of Pb loss ranging from 90% to 99% at 1091.6 Ma, they could give apparent U-Pb dates of 1091.8 Ma (Fig. SI6). However, were the zircons crystallized in the Paleoproterozoic and experienced the same range of Pb loss, discordant U-Pb dates with much older ages than is observed would be expected (Fig. SI6).

Pb diffusion modeling shows that having a population of zircons that crystallized *ca.* 1096 Ma, but subsequently underwent variable degrees of Pb loss between 90% to 99% at 1091.6 Ma would have an apparent U-Pb age of 1091.8 Ma (Fig. SI6). Therefore, based on the U-Pb systematics we cannot rule out the scenario where the Beaver River anorthosite xenoliths crystallized during the Duluth Complex time. However, re-equilibration of Dy elemental zoning throughout zircon grains is expected if 90% Pb loss occurred. Given that our CL images show sharp boundaries between bright and dark zones which are dominantly attributed to the variation in Dy concentrations, it is unlikely that the zircons from anorthosite AX16 experienced intense heating after initial crystallization.

Beaver River diabase structural correction

Structural measurements were obtained from the published geologic maps of the study area. We calculated the mean directions from the combined volcanic bedding measurements from the Schroeder-Lutsen basalt and igneous layering measurements from the Beaver River diabase and constructed two sets of tilt correction data for the paleomagnetic sites in the southern and eastern Beaver Bay Complex (Boerboom, 2004; Boerboom and Green, 2006; Boerboom et al., 2006, 2007; Miller et al., 2001). The mean dip angle for the two areas are very similar while the dip trends are different, with the southern Beaver Bay Complex showing a slightly more easterly trend than the eastern Beaver Bay Complex. This difference in dip trend reflects the overall arcuate shape of the Beaver Bay Complex intrusions along the shore of Lake Superior.

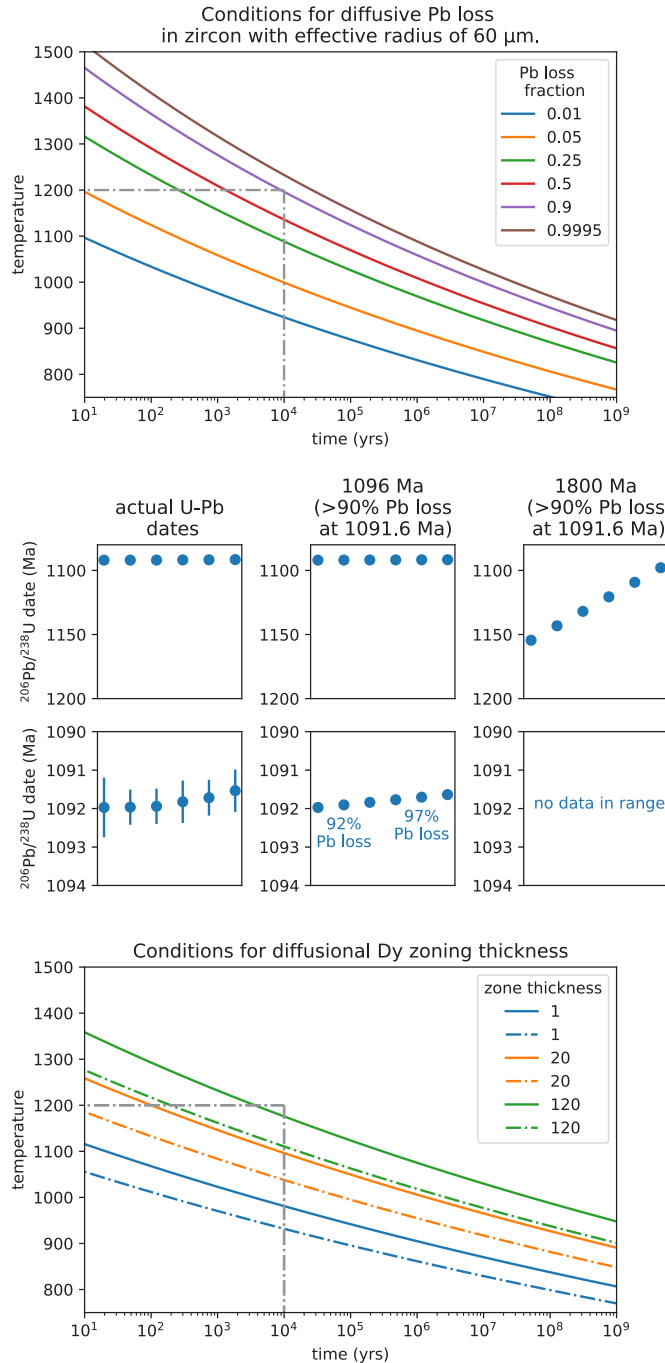


Figure SI6. Top: Conditions for diffusive Pb loss in crystalline zircon for zircons of effective radii of 60 μm . Curves represent time-temperature conditions under which zircon will lose the indicated fraction of total Pb; Middle: Modeled zircon Pb loss scenarios with initial crystallization of 1091.8 Ma, 1096 Ma, and 1800 Ma ages with varying degrees of Pb loss at 1091.6 Ma compared to the actual U-Pb dates; Bottom: Preservation of Dy zoning in zircon. Curves represent time-temperature conditions under which different zoning thicknesses would be preserved in zircon. For conditions above the upper solid curves in each group, well-defined zoning will be lost. For conditions above the dashdot lines zones will be partially lost but still retain initial composition in zone center. Pb diffusion and Dy zoning models are replotted from Cherniak et al. (1997).

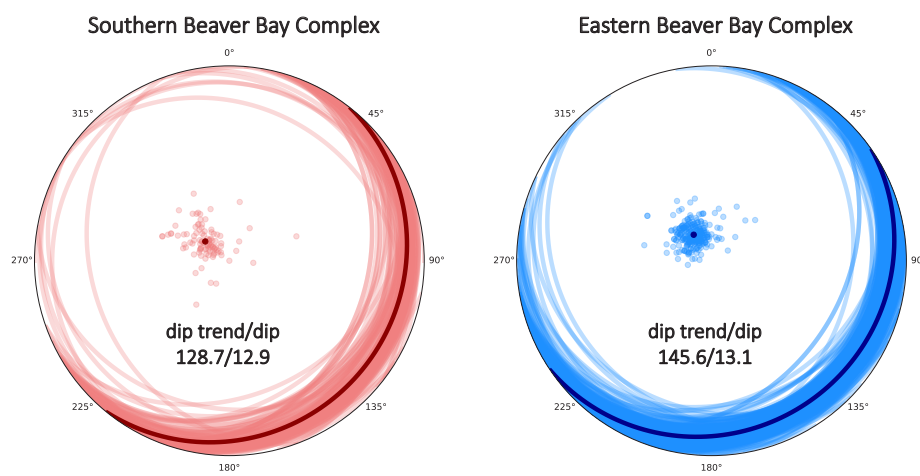


Figure SI7. Stereonet plots of the compiled structural orientation data to tilt correct the paleomagnetic directions obtained from the Beaver River diabase and the anorthositic xenoliths therein.

Table DR2. Zircon chemical abrasion IDTIMS U-Pb isotopic data

Sample	Compositional Parameters						Radiogenic Isotope Ratios						Isotopic Ages							
	Th	$^{206}\text{Pb}^*$	mol %	Pb^*	Pb_c	^{206}Pb	^{208}Pb	^{207}Pb	^{207}Pb	^{235}U	^{238}U	^{206}Pb	corr.	^{207}Pb	^{207}Pb	^{206}Pb	^{206}Pb			
	(a)	U	$\times 10^{-13}$ mol	$^{206}\text{Pb}^*$	Pb_c	(pg)	^{204}Pb	^{206}Pb	^{208}Pb	% err	(e)	(f)	(e)	(f)	(g)	\pm	^{235}U	^{238}U	^{206}Pb	^{206}Pb
(b)	(c)	(c)	(c)	(c)	(c)	(d)	(e)	(e)	(f)	(e)	(f)	(e)	(f)	(g)	(f)	(g)	(g)	(f)	(g)	(f)
MS99033 Anorthosite xenolith in Beaver Bay Diabase (Beaver Bay Complex)																				
z4	0.944	0.8673	0.9977	144	0.17	7696	0.286	0.0759659	0.066	1.93250	0.118	0.184584	0.077	0.856	1093.27	1.31	1092.41	0.79	1091.97	0.77
z8	1.010	6.9857	0.9997	1133	0.18	59449	0.306	0.0759607	0.040	1.93235	0.083	0.184583	0.046	0.974	1093.13	0.81	1092.35	0.56	1091.96	0.46
z1	2.435	6.7175	0.9985	309	0.81	12367	0.738	0.0759449	0.047	1.93191	0.087	0.184579	0.046	0.948	1092.72	0.93	1092.20	0.59	1091.94	0.46
z7	1.008	1.4490	0.9986	239	0.17	12587	0.305	0.0759289	0.056	1.93127	0.098	0.184557	0.055	0.886	1092.30	1.11	1091.98	0.66	1091.82	0.55
z3	1.863	3.3407	0.9992	519	0.22	22932	0.565	0.0759415	0.044	1.93139	0.086	0.184538	0.046	0.950	1092.63	0.89	1092.02	0.58	1091.72	0.47
z6	0.978	0.8594	0.9978	154	0.16	8164	0.296	0.0759062	0.059	1.93015	0.101	0.184504	0.055	0.878	1091.70	1.19	1091.59	0.68	1091.54	0.55
z5	0.971	1.3031	0.9983	196	0.19	10381	0.294	0.0759732	0.056	1.93131	0.095	0.184453	0.050	0.891	1093.46	1.12	1091.99	0.64	1091.26	0.50
z2	0.909	1.7688	0.9985	229	0.22	12318	0.276	0.0759373	0.053	1.93029	0.093	0.184443	0.049	0.910	<u>1092.52</u>	<u>1.06</u>	<u>1091.64</u>	<u>0.62</u>	<u>1091.20</u>	<u>0.49</u>
weighted mean $^{206}\text{Pb}/^{238}\text{U}$ age = 1091.83 \pm <u>0.21 (0.37) [1.15]</u> Ma (2s); MSWD = 0.41 (n=6)																				

(a) z1, z2 etc. are labels for single zircon fragments annealed and chemically abraded after Mattinson (2005); bold indicates analyses used in weighted mean calculations.

(b) Model Th/U ratio iteratively calculated from the radiogenic $^{208}\text{Pb}/^{206}\text{Pb}$ ratio and $^{206}\text{Pb}/^{238}\text{U}$ age.

(c) Pb^* and Pb_c represent radiogenic and common Pb, respectively; mol % $^{206}\text{Pb}^*$ with respect to radiogenic, blank and initial common Pb.

(d) Measured ratio corrected for spike and fractionation only. Fractionation estimated at 0.18 (Daly) or 0.10 (Faraday) \pm 0.02 %/a.m.u. based on analysis of NBS-981 & 982.

(e) Corrected for fractionation, spike, and common Pb; all common Pb was assumed to be procedural blank: $^{206}\text{Pb}/^{204}\text{Pb} = 18.60 \pm 0.72\%$; $^{207}\text{Pb}/^{204}\text{Pb} = 15.69 \pm 0.62\%$; $^{208}\text{Pb}/^{204}\text{Pb} = 38.51 \pm 0.74\%$ (all uncertainties 1-sigma). Isotope dilution measurements made with the ET535 spike (Condon et al., 2015).

(f) Errors are 2-sigma, propagated using the algorithms of Schmitz and Schoene (2007).

(g) Calculations are based on the decay constants of Jaffey et al. (1971). All ratios and ages corrected for initial $^{230}\text{Th}/^{238}\text{U}$ disequilibrium with Th/U [magma] = 3.

References

- Boerboom, T. J., 2004, M-147 Bedrock geology of the Split Rock Point quadrangle, Lake County, Minnesota: Tech. rep., Minnesota Geological Survey.
- Boerboom, T. J., Green, J., and Albers, P., 2007, M-174 Bedrock geology of the Lutsen quadrangle, Cook County, Minnesota: Tech. rep., Minnesota Geological Survey.
- Boerboom, T. J. and Green, J. C., 2006, M-170 Bedrock geology of the Schroeder quadrangle, Cook County, Minnesota: Tech. rep., Minnesota Geological Survey.
- Boerboom, T. J., Green, J. C., Albers, P., and Miller, J., J.D., 2006, M-171 Bedrock geology of the Tofte quadrangle, Cook County, Minnesota: Tech. rep., Minnesota Geological Survey.
- Cherniak, D., Hanchar, J., and Watson, E., 1997, Rare-earth diffusion in zircon: Chemical Geology, vol. 134, pp. 289–301, doi:10.1016/s0009-2541(96)00098-8.
- Cherniak, D. and Watson, E., 2001, Pb diffusion in zircon: Chemical Geology, vol. 172, pp. 5–24, doi:10.1016/s0009-2541(00)00233-3.
- Ferry, J. M. and Watson, E. B., 2007, New thermodynamic models and revised calibrations for the Ti-in-zircon and Zr-in-rutile thermometers: Contributions to Mineralogy and Petrology, vol. 154, pp. 429–437, doi:10.1007/s00410-007-0201-0.
- Gerstenberger, H. and Haase, G., 1997, A highly effective emitter substance for mass spectrometric Pb isotope ratio determinations: Chemical Geology, vol. 136, pp. 309–312.
- Krogh, T., 1973, A low contamination method for the hydrothermal decomposition of zircon and extraction of U and Pb for isotopic age determinations: Geochimica Cosmochimica Acta, vol. 37, pp. 485–494, doi:10.1016/0016-7037(73)90213-5.
- Miller, J., J.D., Severson, M. J., Chandler, V. W., and Peterson, D. M., 2001, M-119 Geologic map of the Duluth Complex and related rocks, northeastern Minnesota: Tech. rep., Minnesota Geological Survey.
- Morrison, D. A., Ashwal, L. D., Phinney, W. C., Shih, C.-Y., and Wooden, J. L., 1983, Pre-Keweenawan anorthosite inclusions in the Keweenawan Beaver Bay and Duluth Complexes, northeastern Minnesota: Geological Society of America Bulletin, vol. 94, p. 206, doi:10.1130/0016-7606(1983)94;206:paiitk;2.0.co;2.
- Sun, S.-S. and McDonough, W. F., 1989, Chemical and isotopic systematics of oceanic basalts: implications for mantle composition and processes: Geological Society, London, Special Publications, vol. 42, pp. 313–345, doi:10.1144/gsl.sp.1989.042.01.19.
- Watson, E. B., Wark, D. A., and Thomas, J. B., 2006, Crystallization thermometers for zircon and rutile: Contributions to Mineralogy and Petrology, vol. 151, pp. 413–433, doi:10.1007/s00410-006-0068-5.